Electronic Supplementary Material (ESI) for Environmental Science: Nano.
This journal is © The Royal Society of Chemistry 2019

SUPPORTING INFORMATION
Comparing TiO_2 Nanoparticle Formulations: Stability and Photoreactivity Are Key Factors in Acute Toxicity to *Daphnia magna*

Jeffrey M. Farner, Rachel Cheong, Emeric Mahé, Hemanshu Anand, Nathalie Tufenkji*

Department of Chemical Engineering, McGill University, Montreal, Quebec, Canada
*Corresponding Author Phone: (514) 398-2999; Fax: (514) 398-6678; E-mail: nathalie.tufenkji@mcgill.ca

Supplementary Data

S1. UV Bulb Output and Model
S2. TiO_2 NP characterization
S3. Terephthalic acid standard curve
S4. UV light attenuation
S5. Daphnia swimming assay

S1. UV Bulb Output and Model

The UV bulb output was modeled as a gaussian distribution ranging from 340 – 390 nm following Jassby et al. [1] with total integrated intensity (Figure S1, bottom) equal to the 13 W m^{-2} used in sample UV exposures.

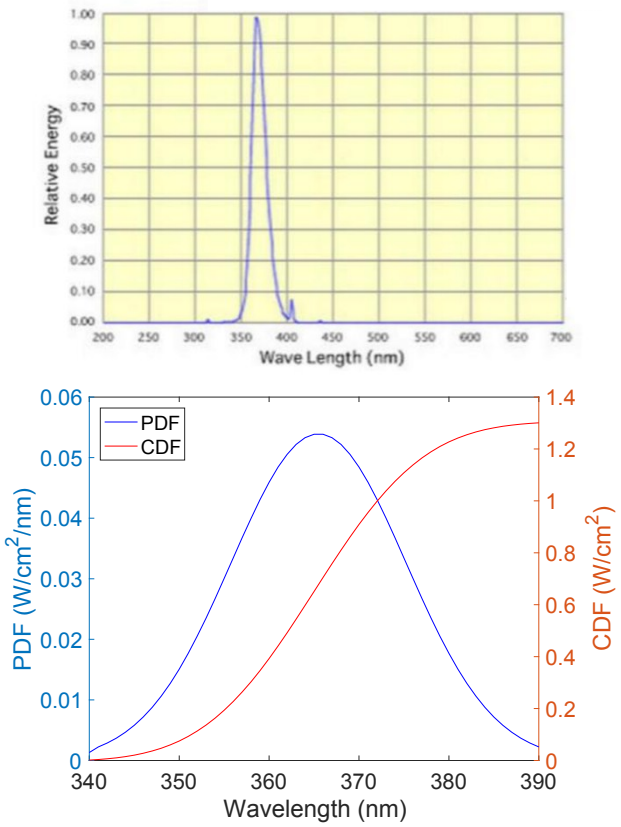

Figure S1. Output spectra of UV bulbs, per manufacturer (top) and modeled as a gaussian distribution (bottom).

S2. TiO_2 NP characterization

Surface analysis was performed on the samples by XPS. Figure S2 shows the survey scans of P25 and CoRI, and Table S1 shows the binding energy for the Ti2p 3/2, O1s and C1s peaks for the NPs. The carbon peak at 286 eV is attributed to the carbon tape.

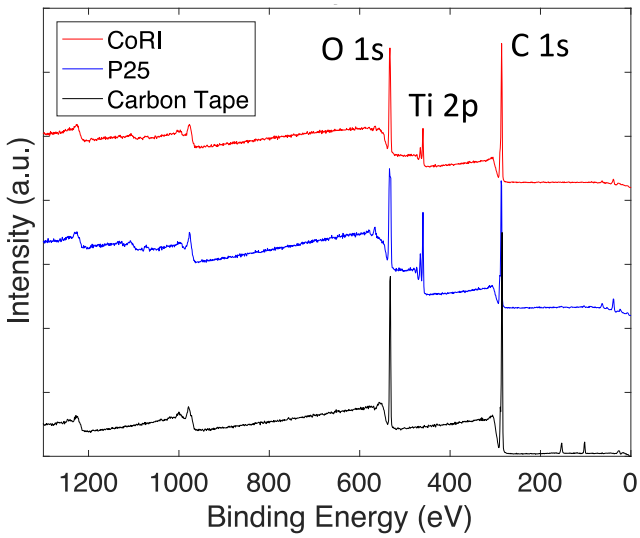

Figure S2. Survey scans of P25 and CoRI NPs.

Table S1. Binding energy for Ti 2p, O 1s and C 1s peaks.

Sample	Ti $2P_{3/2}$ (eV)	O 1s (eV)	C 1s (eV)
P25	460.13	532.49	286.11
CoRI	460.12	533.14	286.12

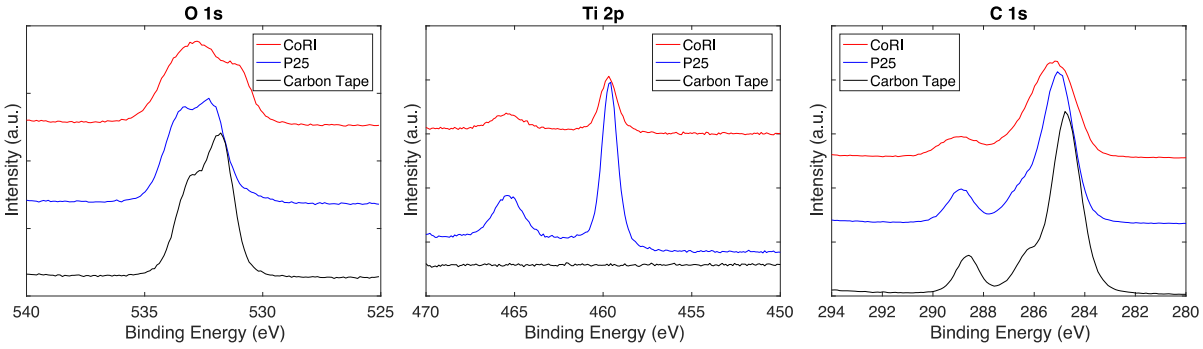

Figure S3. XPS spectra of the O 1s, Ti 2p, and C 1s peaks of P25 and CoRI NPs.

Table S2. Details of SAED patterns for CoRI and P25 compared to literature values. References for diffraction data were taken from the American Mineralogist Crystal Structure Database.

	CoRI	P25	anatase		Literature values for anatase			Literature values for rutile		
	sample	sample	Horn1972[2]	Miller index	Horn1972[2]	Wyckoff1963[3]	Miller index	Swope1995[4]	Meagher1979[5]	Miller index
	d-spacing	d-spacing	d-spacing		d-spacing	d-spacing		d-spacing	d-spacing	
Ring	(angstrom)	(angstrom)	(angstrom)	hkl	(angstrom)	(angstrom)	hkl	(angstrom)	(angstrom)	hkl
1	3.644	3.527	3.5163	101	3.5163	3.5169	101	3.2435	3.2477	110
2	2.430	2.377	2.3786	004	2.4307	2.4309	103	2.4836	2.4875	101
3	1.988	1.918	1.8921	200	2.3786	2.3785	004	2.2935	2.2965	200
4	1.735	1.708	1.7001	105	2.3322	2.3326	112	2.1840	2.1873	111
5	1.540	1.508	1.4931	213	1.8921	1.8925	200	2.0514	2.0541	210
6	1.402	1.367	1.3642	116	1.7001	1.7001	105	1.6849	1.6874	211
7	1.317	1.271	1.2646	215	1.6662	1.6665	211	1.6217	1.6239	220
8	1.215	1.176	1.1661	224	1.4931	1.4933	213	1.4770	1.4795	002
					1.4808	1.4809	204	1.4505	1.4524	310
					1.3642	1.3642	116	1.3579	1.3598	301
					1.3379	1.3382	220	1.3442	1.3464	112
					1.2646	1.2647	215	1.3020	1.3038	311
					1.2505	1.2507	301	1.2418	1.2437	202
					1.1661	1.1663	224	1.1986	1.2005	212
					1.1605	1.1607	312	1.1685	1.1700	321
								1.1467	1.1482	400

Table S3. Details of DLS measurements for NP suspension characterization

Sample	Z-Ave	PdI	Pk 1 Mean Int	Pk 1 Area Int	Pk 2 Mean Int	Pk 2 Area Int	Pk 3 Mean Int	Pk 3 Area Int
	d.nm		d.nm	Percent	d.nm	Percent	d.nm	Percent
P25	164.7	0.227	160.4	100	0	0	0	0
P25	167.2	0.184	191.2	100	0	0	0	0
P25	169.9	0.223	216.6	98.2	28.97	1.6	13.83	0.2
P25 + NOM	138.7	0.209	135.3	100	0	0	0	0
P25 + NOM	139.1	0.189	147.3	97.8	4971	2.2	0	0
P25 + NOM	146.8	0.259	148.2	96.8	5180	3.2	0	0
CoRI	2127	1	305.3	100	0	0	0	0
CoRI	1491	0.59	620.4	100	0	0	0	0
CoRI	1179	0.622	560.2	100	0	0	0	0
CoRI + NOM	4393	1	85.7	100	0	0	0	0
CoRI + NOM	1609	1	438.8	100	0	0	0	0
CoRI + NOM	1400	0.459	612.3	100	0	0	0	0

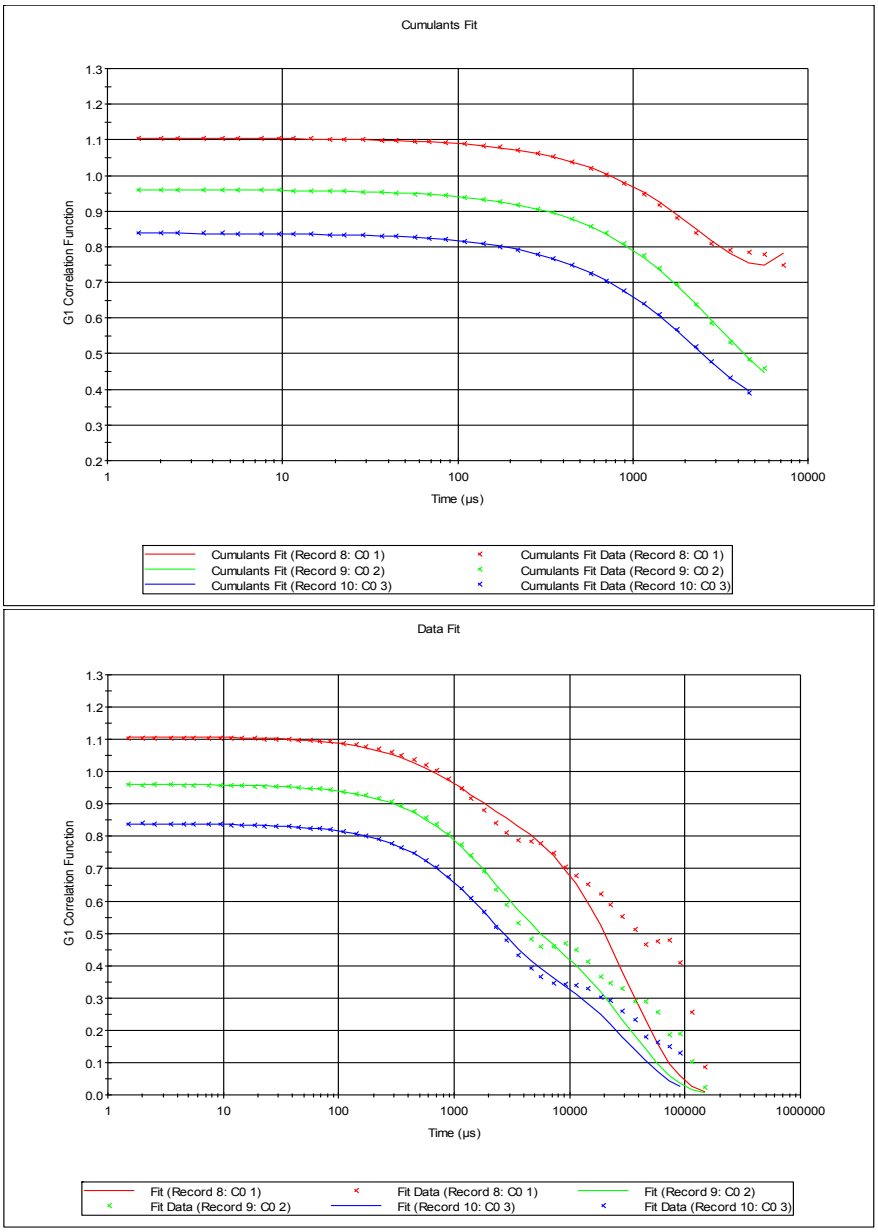

Figure S4. Cumulants Fit and Data Fit plots for CoRI suspensions from Zetasizer software. Note the poor fit at higher times, especially for the Data Fit curve (left), which includes larger aggregates.

The Zetasizer software uses the Cumulant Fit plot to calculate the intensity weighted mean aggregate size (Z-Average and PDI) [6]. The Data Fit plot is used to calculate the distribution analysis, here using Non-Negative Least Squares analysis (general purpose mode). Figure S4 shows these fits for CoRI suspensions listed in Table S2. The ZetaSizer Nano ZS software calculates the Z-average diameter by fitting a single value to the cumulants fit. The intensity weighted results are achieved through the distribution analysis, which includes longer times and will return multiple results for polydisperse data in order to minimize the cumulant residual. As a result, multiple modes are calculated and the impact of the largest aggregates that are less accurately modeled by the software is minimized. For monodisperse samples, the Z-average and intensity weighted average results will be the same [7]. Samples for which large differences between the Z-average and the intensity weighted average exist are often associated with high polydispersity indexes.

Determination of the Isoelectric Point (IEP) for each NP formulation was performed in duplicate by measuring the electrophoretic mobility versus pH. Suspension were continually stirred, and pH was adjusted with HCl. Results are given in Figure S5.

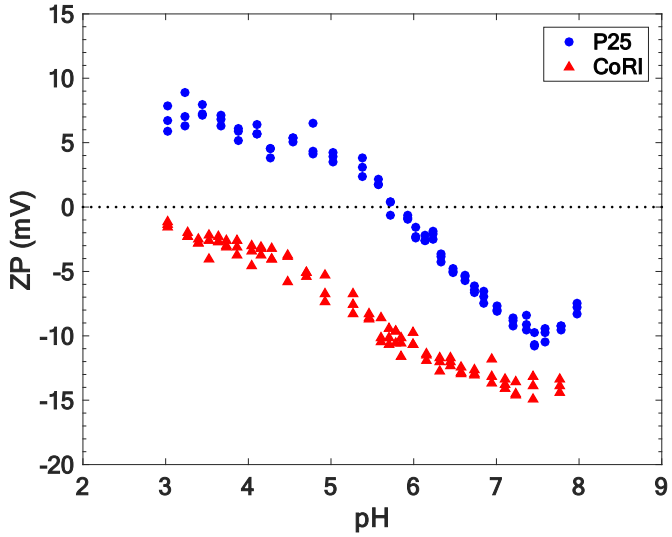

Figure S5. ZP (mV) versus pH for P25 and CoRI. The IEP for P25 is roughly 5.8, while that for CoRI was not observed.

Derived count rates (in kilocounts per second) were taken from TR-DLS measurements of aggregates in suspension over 48 h for P25 and CoRI in the presence or absence of NOM. Count rates refer to the number of scattered photons hitting the detector. As aggregates settle, there are fewer instances of incident photons being reflected, resulting in a decrease in the count rate. As can be seen in Figure S6, this is most pronounced for CoRI, CORI + NOM, and P25; conditions where NPs are least stable.

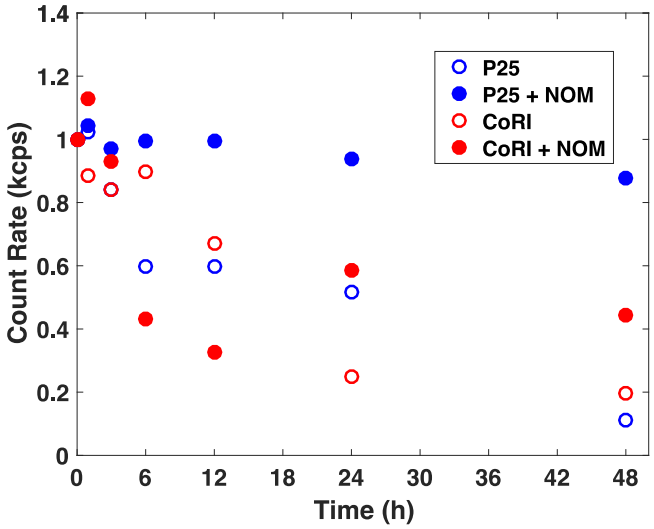

Figure S6. Count rate (kcps) versus time for P25 and CoRI in the presence or absence of NOM.

Calculations of Stokes' settling velocity performed to understand the likelihood of aggregates to settle over 48 h. Aliquots of TiO_2 NP suspensions measured by ICP/MS were taken at mid-

height (6.9 cm) in the polypropylene beakers used throughout the study. Figure S7 shows the radii of spherical particles that will travel the full height (13.8 cm) and mid-height of the water column over 48 h according to the equation for Stokes' settling velocity,

$$V = \frac{2(\rho_p - \rho_f) g\, r^2}{9\,\mu} \qquad \text{(Eq S1)}$$

where V is the settling velocity, ρ_p is the density of the particle (4230 kg / m^3), ρ_f is the density of the fluid (1000 kg / m^3), g is the gravitational constant, r is the radius, and μ is the kinematic viscosity of water (0.001 kg / m s). Assuming the settling velocity is quickly reached, Equation S1 can be rearranged to calculate the time, t, necessary to travel a given distance, d, as a function of particle radius,

$$t = \frac{9\,\mu\, d}{2(\rho_p - \rho_f) g\, r^2} \qquad \text{(Eq S2)}$$

Plotting t vs. r for distances of 13.8 and 6.9 cm yields Figure S7.

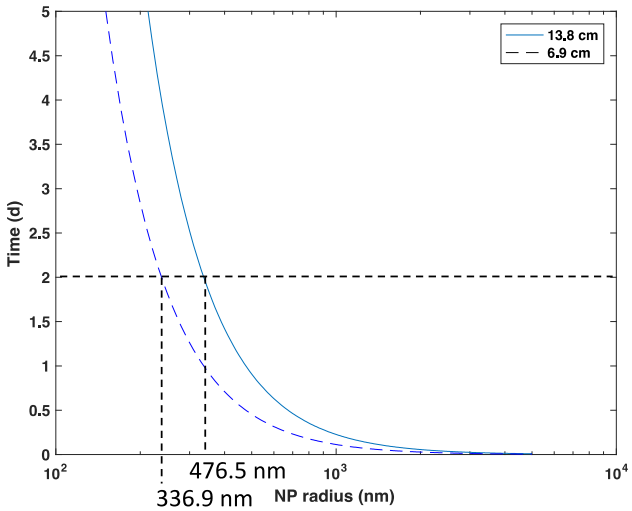

Figure S7. Time (d) required to settle either 13.8 cm (solid blue line) or 6.9 cm (dashed blue line) versus NP radius (nm) calculated from Stoke's settling velocity

S3. Terephthalic acid standard curve

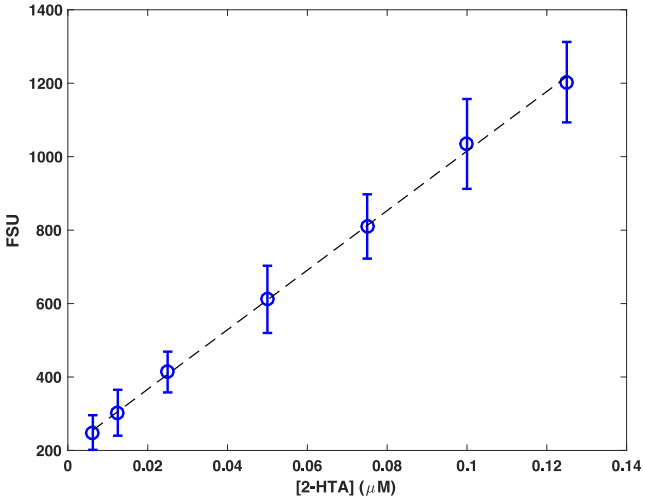

Figure S8. Standard curve indicating linear response of fluorescence (FSU) versus 2-HTA concentration (μM).

The standard curve for *OH quantification was created by measuring fluorescence of 2-HTA versus concentration (0.00625 – 0.125 μM), shown in Figure S8. The response was linear over the measured concentration range with a calculated R^2= 0.999. To determine the rate of *OH generation in samples, the least squares fit of cumulative fluorescence (Figure S9) was converted to 2-HTA concentration, assuming that the *OH trapping efficiency of TA is 80% [8]. Fluorescence measurements that resulted in less than the minimum 2-HTA response (the minimum quantification limit, 0.00625 μM 2-HTA = 250 FSU) are indicated as < MQL.

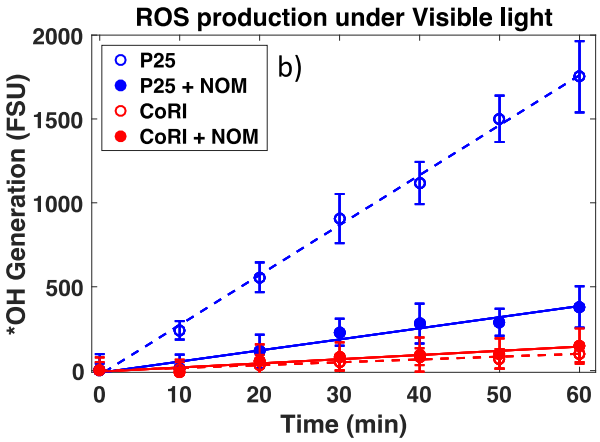

Figure S9. Cumulative fluorescence (FSU) versus time for 10 ppm CoRI in the presence or absence of NOM illuminated by visible light.

S4. UV light attenuation

UV light attenuation was based on the modeled bulb output (Figure S1). Given from the Beer-Lambert law that

$$ABS(\lambda) = -\log\frac{I(\lambda)}{I(\lambda)_o} = \epsilon(\lambda)\, c\, l \qquad \text{(Eq S3)}$$

Where l = 1 cm and c is the concentration of, e.g., NOM, the absorptivity of NOM for each wavelength, $\epsilon(\lambda)_{NOM}$ in units of L mg^{-1} cm^{-1} was obtained from ABS measurements with a UV-Vis spectrophotometer (Agilent 8453). Measurements used a 1 cm path length quartz cuvette with DI water as the blank. ABS of NOM concentrations ranging from 100 to 1.25 ppm were measured and the molar absorptivity was determined for each wavelength across the range of modeled bulb output (340 – 390 nm).

The absorption coefficient, $\alpha(\lambda)$, of NOM in units of cm^{-1} was calculated following:

$$\alpha(\lambda) = \epsilon(\lambda)\, c \qquad \text{(Eq S4)}$$

Assuming that UV light attenuation exists in the system due to DI water, the ions present in MHW, and NOM, the various absorption coefficients can be used to determine the intensity of light as a function of depth in the beaker by combining Equations S3 and S4 to

$$I(\lambda) = I(\lambda)_o 10^{-\left(\alpha(\lambda)_{NOM} + \alpha(\lambda)_{DI} + \alpha(\lambda)_{IONS}\right)l} \qquad \text{(Eq S5)}$$

where $I(\lambda)_o$ is the modeled bulb output, $\alpha(\lambda)_{DI}$ and $\alpha(\lambda)_{IONS}$ are the absorption coefficients of DI water and the ions present in MHW, respectively, and l is the depth of the water column (ranging from 0 cm at the upper liquid surface to 13.8 cm). To more accurately describe the loss of intensity due to DI water, we combine the absorbance and scattering values reported by Buiteveld et al. [9] to produce extinction coefficients, $\varepsilon(\lambda)_{DI}$. These values are quite close to $\alpha(\lambda)_{DI}$values reported by Sogandares and Fry [10] and Belmont et al. [11].

Values for $\alpha(\lambda)_{IONS}$ were obtained in a similar manner to NOM, with the ABS spectra of MHW recorded in a quartz cuvette and using DI water as a blank. Because of the extremely low ABS values, there is considerable noise in $\alpha(\lambda)_{IONS}$ values, including negative values. As can be seen in Figure S10, values for $\varepsilon(\lambda)_{DI}$ and $\alpha(\lambda)_{IONS}$ are on the same order of magnitude as each other and two orders of magnitude lower than $\alpha(\lambda)_{NOM}$. Thus, for NOM containing samples, the relative impact of MHW is negligible and only $\alpha(\lambda)_{NOM}$ is considered. For samples that do not contain NOM, $\varepsilon(\lambda)_{DI}$ and $\alpha(\lambda)_{IONS}$, become the primary cause of attenuation. Given the uncertainty in $\alpha(\lambda)_{IONS}$ and similar magnitude between the two, $\alpha(\lambda)_{IONS}$ was assumed equal to $\alpha(\lambda)_{NOM}$ for calculations.

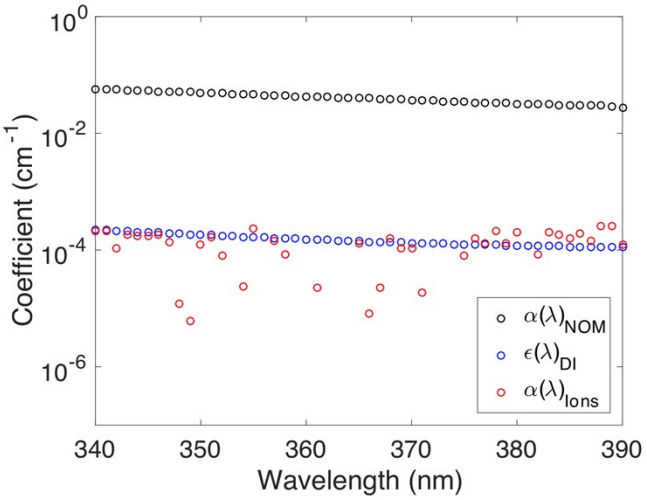

Figure S10. Absorption coefficients versus wavelength for DI water [9], 10 ppm NOM (measured), and MHW (Ions, measured).

Using Equation S5 and integrating across the wavelengths (340 – 390 nm), the light intensity was calculated as a function of depth, shown in Figure S10. As can be seen, the UV intensity only changes by 0.5 % across the beaker depth in MHW due to DI water and the ionic makeup of MHW. In the presence of NOM, however, the total intensity of UV light at the bottom of the beaker, at 3.7 W m^{-2}, is 28.5 % that of the upper surface. By integrating Equation S5 over the distance of the beaker, the calculated intensity at half height in the water column is 6.9 W m^{-2}, and the average UV light intensity is 7.4 W m^{-2}. Note that, even using values from Buiteveld et al., the contribution from MHW ($\varepsilon(\lambda)_{DI} + \alpha(\lambda)_{IONS}$,) is minimal, as shown in Figure S11.

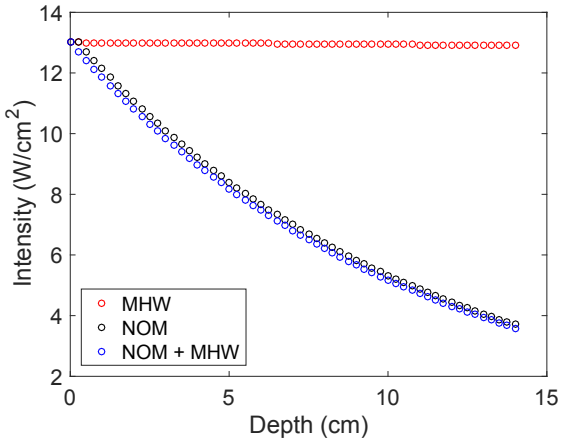

Figure S11. Modeled light intensity as a function of depth in beakers for NOM, DI + ions (MHW), and all three constituents (NOM + MHW).

S5. *Daphnia* swimming assay

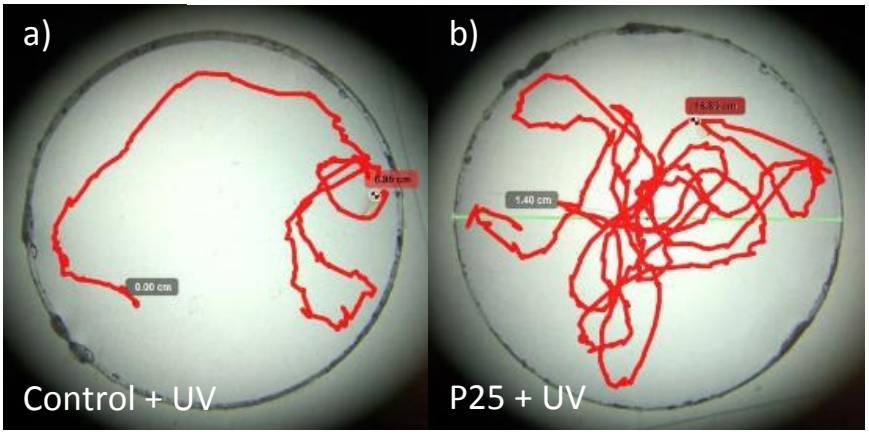

Figure S12. Representative swimming traces after 1 min for *D. magna* in a) control and b) P25 exposed to UV light as determined using the Kinovea software.

References

1. Jassby, D.; Budarz, J. F.; Wiesner, M., Impact of Aggregate Size and Structure on the Photocatalytic Properties of TiO2 and ZnO Nanoparticles. *Environ Sci Technol* **2012,** *46*, (13), 6934-6941.
2. Horn, M.; Schwebdtfeger, C.; Meagher, E., Refinement of the structure of anatase at several temperatures. *Zeitschrift für Kristallographie-Crystalline Materials* **1972,** *136*, (1-6), 273-281.
3. Wyckoff, R., Crystal Structures, Interscience. *New York* **1963,** *1*, 254.
4. Swope, R. J.; Smyth, J. R.; Larson, A. C., H in rutile-type compounds: I. Single-crystal neutron and X-ray diffraction study of H in rutile. *American Mineralogist* **1995,** *80*, (5-6), 448-453.
5. Meagher, E.; Lager, G. A., Polyhedral thermal expansion in the TiO 2 polymorphs; refinement of the crystal structures of rutile and brookite at high temperature. *The Canadian Mineralogist* **1979,** *17*, (1), 77-85.
6. Malvern, I., Inform white paper dynamic light scattering. *Malvern: Malvern Instruments Ltd* **2011**, 1-6.
7. Bhattacharjee, S., DLS and zeta potential–What they are and what they are not? *Journal of Controlled Release* **2016,** *235*, 337-351.
8. Ishibashi, K.-i.; Fujishima, A.; Watanabe, T.; Hashimoto, K., Quantum yields of active oxidative species formed on TiO2 photocatalyst. *Journal of Photochemistry and Photobiology A: Chemistry* **2000,** *134*, (1), 139-142.
9. Buiteveld, H.; Hakvoort, J.; Donze, M. In *Optical properties of pure water*, Ocean Optics XII, 1994; International Society for Optics and Photonics: 1994; pp 174-184.
10. Sogandares, F. M.; Fry, E. S., Absorption spectrum (340–640 nm) of pure water. I. Photothermal measurements. *Applied Optics* **1997,** *36*, (33), 8699-8709.

11. Belmont, P.; Hargreaves, B. R.; Morris, D. P.; Williamson, C. E., Estimating attenuation of ultraviolet radiation in streams: field and laboratory methods. *Photochemistry and photobiology* **2007,** *83*, (6), 1339-1347.